Available online at www.sciencedirect.com
ScienceDirect
International Journal of Heat and Mass Transfer 50 (2007) 3461–3470
International Journal of HEAT and MASS TRANSFER
www.elsevier.com/locate/ijhmt

Modeling of ultrashort laser pulse-train processing of metal thin films

Lan Jiang [a,b], Hai-Lung Tsai [b,*]

[a] Department of Mechanical and Automation Engineering, 3rd School, Beijing Institute of Technology, 100081, PR China
[b] Laser-Based Manufacturing Laboratory, Department of Mechanical and Aerospace Engineering, University of Missouri-Rolla, Rolla, MO 65409, United States

Received 27 January 2006; received in revised form 12 January 2007
Available online 6 April 2007

Abstract

The improved two-temperature model with quantum treatments is used to analyze the ultrashort laser pulse-train processing of gold thin films. This study demonstrates that (1) as compared to "normal" laser heating, pulse-train technology can increase the photon efficiency, i.e., less total laser energy is required to achieve the same lattice temperature or phase change; (2) the number of bursts required for melting decreases with the repetition rate, but at tens of MHz or higher, the repetition rate has a negligible effect; (3) the lattice temperature at the thermolization time first increases to a peak and then decreases as the pulse separation time increases.

Keywords: Ultrashort laser pulses; Pulse-train; Thin film processing

1. Introduction

In the past two decades, the ultrashort (typically <10 ps) laser heating of metals and its non-equilibrium energy transport have been very active research topics [1–10,4,11–17]. Particularly, special attention has been paid to the femtosecond laser heating of thin films [2,5–9,12–15]. Recent developments of optical devices make it possible to obtain almost any arbitrary pulse shapes. A pulse train consists of "bursts" or "trains" at a separation time of a few miniseconds to microseconds, and each burst may contain multiple pulses at a separation time of 100 of femtoseconds to a few picoseconds. A large number of studies have been reported regarding pulse shaping and its effects on laser-material interactions [18–28]. For example, using a shaped pulse train, ionization process can be controlled [18]; atoms can be selectively ionized [19]; molecular ground-state rotational dynamics can be manipulated [20]; chemical reactions can be controlled [21]; and X-ray line emission from plasmas under the femtosecond pulse can be significantly enhanced [22]. These abilities of shaped pulse trains are useful to control and improve micro-/nano-scale processing of dielectrics [23,24], semiconductors [25], and metals [26–28].

In the past, the well known two-temperature model has been widely used for the ultrashort laser processing of metals [2,5–9,12–15]. However, in the existing two-temperature model, the estimations for the important properties such as electron heat capacity, electron relaxation time, electron heat conductivity, and reflectivity are limited to temperatures much lower than the Fermi temperature [8]. Using the improved two-temperature model in which the quantum treatments were employed to calculate the significantly varying properties [2], this study investigates the pulse train technology, especially the effects of the pulse number per train, pulse separation, and repetition rate for gold thin films.

2. Mathematical model

2.1. Two-temperature model

Using the improved two-temperature model [2], this paper considers the laser pulse durations that are much

* Corresponding author. Tel.: +1 573 341 4945; fax: +1 573 341 4607.
E-mail address: tsai@umr.edu (H.-L. Tsai).

0017-9310/$ - see front matter © 2007 Elsevier Ltd. All rights reserved.
doi:10.1016/j.ijheatmasstransfer.2007.01.049

Nomenclature

B	bulk modulus
b_{max}	maximum collision parameter in Eq. (14)
b_{min}	minimum collision parameter in Eq. (14)
c	speed of light in vacuum
$\mathbf{c}$	velocity of light in vacuum
C	heat capacity
C_e	electron heat capacity
C_l	lattice heat capacity
c_s	speed of sound
d	film thickness
e	electron charge
$\mathbf{f}$	complex refractive index
f_1	normal refractive index
f_2	extinction coefficient
$F_{1/2}$	Fermi integral
G	electron-lattice coupling factor
h	Planck constant
$\hbar$	reduced Planck constant
I	laser intensity
F	laser fluence in J/cm^2
k	heat conductivity
k_B	Boltzmann's constant
k_e	electron conductivity
k_l	metal heat conductivity in the electron–phonon thermal equilibrium
m_e	mass of electron
n_e	density of the free electrons
$\langle n_k \rangle$	average number of electrons in energy state ε_k
N_e	total number of free electrons
r	distance to the Gaussian beam axis
r_0	radius of the laser beam
R	reflectivity
R_l	heat loss due to surface irradiation
S	laser source term
S'	laser source term used in existing models [5–8]
t	time
t_p	pulse duration
T_D	Debye temperature
T_e	electron temperature
T_F	Fermi temperature
T_l	lattice temperature
T_0	ambient temperature
T	metal temperature in the electron–phonon thermal equilibrium
$\mathbf{v}$	velocity of light in the material
v_e^2	mean square of electron speed
Z^*	ionization state
z	depth from the thin film surface
V	volume

Greek symbols

α	overall absorption coefficient
α_h	absorption coefficient through heating
δ	optical penetration depth
$\boldsymbol{\epsilon}$	complex dielectric function
ϵ_0	electrical permittivity of free space
ϵ_1	real part of the dielectric function
ϵ_2	imaginary part of the dielectric function
ε	kinetic energy of a free electron
$\langle \varepsilon \rangle$	average electron kinetic energy
$\langle \varepsilon_p \rangle$	average phonon kinetic energy
ε_d	d-band energy
ε_e	the emissivity
ε_F	Fermi energy
ε_k	electron energy state
$\ln \Lambda$	Coulomb logarithm in Eq. (13)
λ	wavelength of the laser
μ	chemical potential
ν	laser frequency
ρ	density of states
ρ_F	distribution of occupied electronic states
ρ_m	density
σ	Stefan–Boltzmann constant
τ_e	electron relaxation time
ω	laser frequency
ω_p	plasma frequency

longer than the electron relaxation time (typically sub to tens of femtoseconds). Hence, the electron temperature, characterized by the Fermi distribution, is well defined and can be employed [1]. The two-temperature model is given below:

$$C_e(T_e)\frac{\partial T_e(t,r,z)}{\partial t} = \nabla \cdot (k_e(T_e)\nabla T_e) - G(T_e - T_l) + S(t,r,z) \tag{1}$$

$$C_l\frac{\partial T_l(t,r,z)}{\partial t} = \nabla(k_l \nabla T_l) + G(T_e - T_l) - R_l \tag{2}$$

where C_e *is* electron heat capacity; C_l is the lattice heat capacity; T_e is the electron temperature; T_l is the lattice temperature; k_e is the electron conductivity; k_l is the metal heat conductivity when the electron–phonon is in thermal equilibrium; t is the time; r is the distance to the Gaussian beam axis; z is the depth from the thin film surface; S represents the laser source term; R_l is the heat loss due to surface irradiation; and G is the electron-lattice coupling factor estimated by [5]

$$G = \frac{\pi^2 m_e n_e c_s^2}{6\tau_e(T_e)T_e(t,r,z)} \tag{3}$$

where m_e is the mass of electron; n_e is the density of the free electrons; τ_e is electron relaxation time; and c_s is the speed of sound in bulk material calculated by

$$c_s = \sqrt{\frac{B}{\rho_m}} \tag{4}$$

where B is the bulk modulus and ρ_m is the density.

2.2. Free electron heat capacity

In a wide range of electron temperatures, the full-run quantum treatment should be used to calculate the free electron heat capacity. In spite of the non-equilibrium states of the electrons within the free electron relaxation time, the Fermi distribution and the corresponding temperature of the free electrons can still be used in the limit when the pulse duration is much longer than the electron relaxation time, which is proved by a model using the full Boltzmann transport theory [1]. The average number of electrons, $\langle n_k \rangle$, in energy state, ε_k, obeys the following Fermi distribution

$$\langle n_k \rangle = \frac{1}{e^{\beta(T_e)(\varepsilon_k - \mu(T_e))} + 1} \tag{5}$$

where $\beta(T_e) = 1/k_B T_e(t,r,z)$, μ is the chemical potential, and k_B is the Boltzmann's constant. For free electron gas, the chemical potential can be calculated by [29]

$$\mu(n_e, T_e) = \varepsilon_F(n_e) \times \left[1 - \frac{\pi^2}{12}\left(\frac{k_B T_e(t,r,z)}{\varepsilon_F(n_e)}\right)^2 + \frac{\pi^2}{80}\left(\frac{k_B T_e(t,r,z)}{\varepsilon_F(n_e)}\right)^4\right] \tag{6}$$

where the higher order terms are neglected and ε_F is the Fermi energy. The Fermi energy is determined by [29]

$$\varepsilon_F = \left(\frac{(hc)^2}{8 m_e c^2}\right)\left(\frac{3}{\pi}\right)^{2/3} n_e^{2/3} \tag{7}$$

where h is the Planck constant and c is the speed of light in vacuum. The average kinetic energy per electron in J, $\langle \varepsilon \rangle$, is calculated by

$$\langle \varepsilon \rangle = \frac{\sum_k \langle n_k \rangle \varepsilon_k}{N_e} = \frac{\int_0^\infty \frac{1}{e^{\beta(T_e)(\varepsilon - \mu(T_e))}+1}\rho(\varepsilon)\varepsilon \, d\varepsilon}{\int_0^\infty \frac{1}{e^{\beta(T_e)(\varepsilon - \mu(T_e))}+1}\rho(\varepsilon) \, d\varepsilon} \tag{8}$$

where ε is the kinetic energy of a free electron; N_e is the total number of free electrons; and $\rho(\varepsilon)$ is the density of states given by

$$\rho(\varepsilon) = \frac{8\sqrt{2}\pi m_e^{3/2}}{h^3}\sqrt{\varepsilon} \tag{9}$$

The heat capacity can be determined by

$$C_e(T_e) = n_e\left(\frac{\partial \langle \varepsilon \rangle}{\partial T_e}\right)_V \tag{10}$$

where V is the volume.

The phonon heat capacity is also temperature-dependent which, in Ref. [2], is calculated by the well-known quantum treatment, the Debye model. However, at temperatures higher than the Debye temperature (165 K for gold), the variation of gold phonon heat capacity is insignificant [2]. At room temperature or higher, for gold phonons, the molar phonon heat capacity predicted by the quantum treatment (the Debye model) is similar to that predicted by the classical estimation (the Law of Dulong and Petit) [2]. Hence, the lattice heat capacity of gold in the calculation is reasonably considered as a constant in this paper.

2.3. Free electron heat conductivity and relaxation time

The free electron heat conductivity is expressed by the following Drude theory of metals [29]

$$k_e(T_e) = \frac{1}{3} v_e^2(T_e)\tau_e(T_e)C_e(T_e) \tag{11}$$

where v_e^2 is the mean square of electron speed. In this study, v_e^2 and C_e are determined directly by the Fermi distribution based on Eqs. (5)–(10). In Eq. (11), the scattering effects are indirectly considered through the calculation of the free electron relaxation time. In $T_D < T_e < 0.1\ T_F$ and using the values of v_e^2 and C_e for an ideal gas, Eq. (11) can be simplified to $\tau_e = \frac{3m_e}{\pi^2 n_e k_B^2 T_e(t,r,z)} k_e(T_e)$ [29] that is used in Ref. [7]. Regarding the temperature range, T_D is the Debye temperature that is 165 K for gold and T_F is the Fermi temperature that is measured to be 5.9×10^4 K for gold.

In this study, by considering metals as dense plasma [1,2,29–34], the free electron relaxation time is calculated as follows by a quantum treatment derived from the Boltzmann transport equation [32,33]

$$\tau_e(t,r,z) = \frac{3\sqrt{m_e}(k_B T_e(t,r,z))^{3/2}}{2\sqrt{2}\pi (Z^*)^2 n_e e^4 \ln\Lambda} \times (1 + \exp(-\mu(T_e)/k_B T_e(t,r,z)))F_{1/2} \tag{12}$$

where e is the electron charge; Z^* is the ionization state and is 1 for gold; $F_{1/2}$ is the Fermi integral; and $\ln\Lambda$ is the Coulomb logarithm determined by

$$\ln\Lambda = \frac{1}{2}\ln\left(1 + \left(\frac{b_{max}}{b_{min}}\right)^2\right) \tag{13}$$

where the maximum (b_{max}) and minimum (b_{min}) collision parameters are given by

$$b_{max} = \frac{(k_B T_e(t,r,z)/m_e)^{1/2}}{\max(\omega, \omega_p)}$$
$$b_{min} = \max\left(\frac{Z^* e^2}{k_B T_e(t,r,z)}, \frac{\hbar}{(m_e k_B T_e(t,r,z))^{1/2}}\right) \tag{14}$$

where $\hbar = h/2\pi$ is the reduced Planck constant; ω is the laser frequency and ω_p is the plasma frequency defined by

$$\omega_p \sqrt{\frac{n_e e^2}{m_e \epsilon_0}} \tag{15}$$

where ϵ_0 is the electrical permittivity of free space.

2.4. Optical properties

A critical task is to determine the laser source term in Eq. (1). A general expression for laser intensity (W/cm^2), I, inside the bulk material for both non-linear and linear absorptions is [32,33]

$$I(t,r,z) = \frac{2F}{\sqrt{\pi/\ln 2}t_p}(1-R(t,r)) \times \exp\left(-\frac{r^2}{r_0^2} - (4\ln 2)\left(\frac{t}{t_p}\right)^2 - \int_0^z \alpha(t,r,z)\,dz\right) \tag{16}$$

where F is the laser fluence in J/cm^2; t_p is the pulse duration; R is the reflectivity; r_0 is the radius of the laser beam that is defined as the distance from the center at which the intensity drops to $1/e^2$ of the maximum intensity; and $\alpha(t,r,z)$ is the absorption coefficient. $S(t,r,z) = \partial I(t,r,z)/\partial z$. If the absorption coefficient is assumed to be a constant, using the definition that optical penetration depth $\delta = 1/\alpha$, the laser source term (W/cm^{-3}) is simplified to the following expression commonly used in the existing models [5–8]

$$S'(t,r,z) = \frac{0.94F}{t_p\delta}(1-R(t,r))\exp\left(-\frac{r^2}{r_0^2} - 2.77\left(\frac{t}{t_p}\right)^2 - \frac{z}{\delta}\right) \tag{17}$$

Rethfeld et al. have demonstrated that the ultrashort laser–metal interaction can be well described by laser–plasma interactions [1]. According to the Drude model for free electrons, ϵ, the electrical permittivity (dielectric function) of metals modeled as a plasma, is expressed as [34]

$$\epsilon(t,r,z) = \epsilon_1(t,r,z) + i\epsilon_2(t,r,z) = \left(1 - \frac{\omega_p^2(n_e)\tau_e^2(t,r,z)}{1+\omega^2\tau_e^2(t,r,z)}\right) + i\left(\frac{\omega_p^2(n_e)\tau_e(t,r,z)}{\omega(1+\omega^2\tau_e^2(t,r,z))}\right) \tag{18}$$

Eq. (18) shows how the plasma frequency in Eq. (15) is defined. The relationship between the complex refractive index, $\mathbf{f}$, and the complex electrical permittivity is given by

$$\left(\frac{\mathbf{c}}{\mathbf{v}}\right) = \mathbf{f} = (f_1 + if_2) = \sqrt{\epsilon} = \sqrt{\epsilon_1 + i\epsilon_2} \tag{19}$$

where $\mathbf{c}$ is the velocity of light in vacuum; $\mathbf{v}$ is the velocity of light in the material; f_1 is the normal refractive index; and f_2 is the extinction coefficient. Thus, the f_1 and f_2 functions can be express as

$$f_1(t,r,z) = \sqrt{\frac{\epsilon_1(t,r,z) + \sqrt{\epsilon_1^2(t,r,z)+\epsilon_2^2(t,r,z)}}{2}}$$
$$f_2(t,r,z) = \sqrt{\frac{-\epsilon_1(t,r,z) + \sqrt{\epsilon_1^2(t,r,z)+\epsilon_2^2(t,r,z)}}{2}} \tag{20}$$

The reflectivity and the absorption coefficient of the metal are determined by the following Fresnel expression

$$R(t,r) = \frac{(f_1(t,r,0)-1)^2 + f_2^2(t,r,0)}{(f_1(t,r,0)+1)^2 + f_2^2(t,r,0)}$$
$$\alpha_h(t,r,z) = \frac{2\omega f_2(t,r,z)}{c} \tag{21}$$

However, the Drude model for metals, Eq. (18), does not consider the interband transition and the Fermi distribution. For gold, the d-band transition plays a critical role in the optical properties [4,35]. In d-band transition, electrons jump from the top of the d-band to the unoccupied states near the Fermi level in the conduction band (p-band). For noble metals like gold, the contribution of interband absorption to optical properties can be directly added to the Drude model, Eq. (18), for electrical permittivity [36]. Experiments have shown that the transient reflectivity of gold films is directly related to the change in occupation number of electrons near the Fermi energy [35]. The change in occupied state distributions near the Fermi level caused by electron heating is called the Fermi distribution smearing [35]. Eesley et al. estimated the distribution of occupied electronic states near the Fermi energy by [35]

$$\rho_F = \frac{1}{1+\exp\{[h\nu - (\varepsilon_F - \varepsilon_d)]/k_B T_e(t,r,z)\}} \tag{22}$$

where ν is the laser frequency; $(\varepsilon_F - \varepsilon_d) = 2.38$ eV for gold [4] is the difference between the Fermi energy and the d-band energy, ε_d. It is seen the absorption of photon energy, $h\nu$, is directly affected by the d-band transition. The smearing of the electron distribution is given by

$$\Delta\rho_F = \rho_F(h\nu, T_e) - \rho_F(h\nu, T_0) \tag{23}$$

which is linearly proportional to the imaginary component of the electrical permittivity in Eq. (18) [4]

$$\frac{\Delta\epsilon_2}{\epsilon_2} = \frac{\Delta\rho_F}{\rho_F} \tag{24}$$

In Eq. (23), T_0 is the ambient temperature, 300 K [4]. After adding $\Delta\epsilon_2$ to ϵ_2 in Eq. (18), the reflectivity and the absorption coefficient with the consideration of d-band transition can be determined by Eq. (21).

3. Results and discussion

3.1. Single burst

The proposed model is first validated by considering the damage thresholds under single pulse per train. As shown in Fig. 1, the proposed model significantly increases the prediction accuracy of the damage thresholds compared with the existing model [5–7]. At the wavelength of 1053 nm, the damage thresholds of single pulse per train processing of 200 nm film predicted by the proposed model are almost independent of the pulse duration in 140 fs–100 ps, which is confirmed by the experimental data [3].

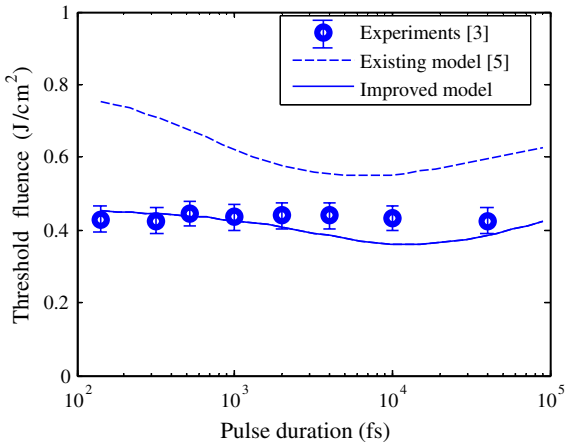

Fig. 1. Damage threshold fluences of 200 nm gold film processed by single pulse per train at the wavelength of 1053 nm and different pulse durations.

Then, using the validated model, this section investigates a 140 fs (t_p), 1053 nm (Λ) laser heating of gold film with the size of 10 mm (width) × 10 mm (length) × 200 nm (thickness) by a single burst consisting of 1, 2, 4, or 10 pulses. Perfect insulation is assumed between the thin film and its substrate in the calculation. Our calculation starts with $-2t_p$, and $t = 0$ corresponds to the peak energy of the first pulse in the train. Fig. 2 compares the electron temperatures and phonon temperatures at the center surface point ($r = 0$; $z = 1$ nm) heated by one burst of four cases: (a) single pulse per train at 0.1 J/cm^2; (b) 2 pulses per train at 0.05 J/cm^2 per pulse; (c) 4 pulses per train at 0.025 J/cm^2 per pulse and (d) 10 pulses per train at 0.01 J/cm^2 per pulse. The pulse separation time between the two next pulses within a train is 1 ps. It is seen the highest electron temperature of each case occurs right after the last pulse in each train due to the incubation effect of the previous pulses, and it is, respectively, 8.9×10^3 K, 7.4×10^3 K, 5.3×10^3 K, and 3.3×10^3 K for Cases (a)–(d). The decrease of the maximum electron temperature is expected, since the laser energy in Case (a) was delivered within 140 fs, as compared to 1.14 ps, 3.14 ps, and 9.14 ps, respectively, in Cases (b)–(d). Hence, at the same total energy per train and same pulse separation time, the non-equilibrium effect between the electrons and phonons is significantly reduced as the number of pulses per train increases. The thermolization times are 12 ps, 12.5 ps, 13 ps, and 17 ps, respectively, for 1, 2, 4, and 10 pulses per train. The pulse train technology tends to reduce the problems associated with thermal cycles, such as stress-fracturing caused by repeated phase changes and their inverse processes. Also, the transient heat conductivity is lowered by the pulse train technology.

The responses of electron temperatures at the depths of 0, 40, 80, 120, and 160 nm are shown in Fig. 3 where the arrows indicate the directions toward which the depth increases. The trends at all the depths are quite similar to each other. The perturbations induced by the femtosecond pulses are significantly weakened as the depth increases, due to the attenuation of transmitted laser energy distribution. Before the thermolization time, the ratio of electron temperature change to time significantly decreases with the increases of the number of pulses per train. This tends to decrease the temperature gradient in space domain and the associated stress especially in the multiple-burst heating process.

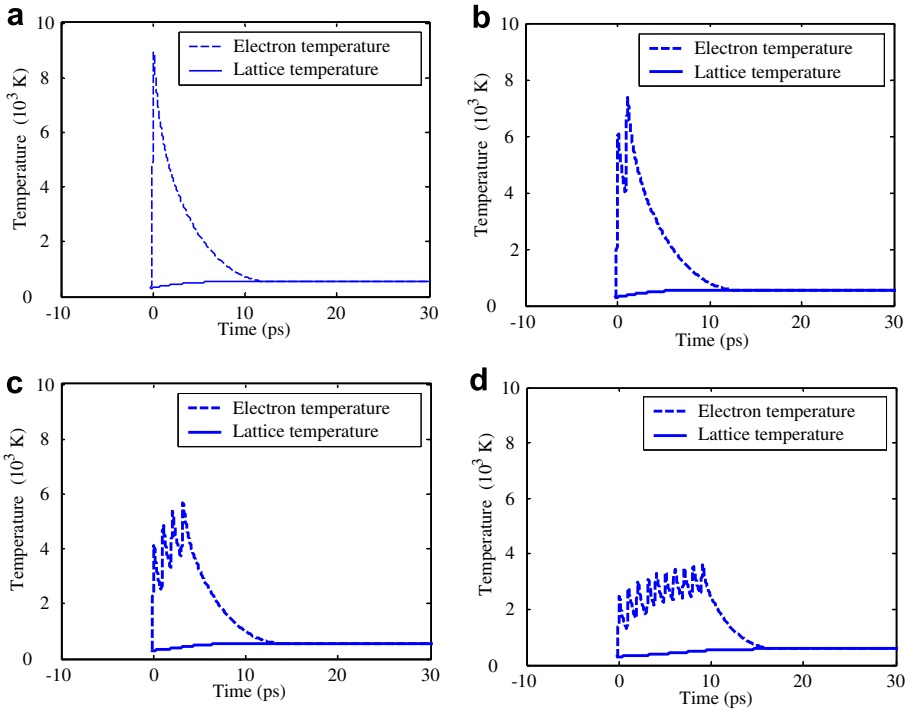

Fig. 2. Surface center ($r = 0$; $z = 1$ nm) temperatures of electrons and phonons (single burst; pulse separation = 1 ps): (a) single pulse per train at 0.1 J/cm^2 per pulse; (b) 2 pulses per train at 0.05 J/cm^2 per pulse; (c) 4 pulses per train at 0.025 J/cm^2 per pulse; (d) 10 pulses per train at 0.01 J/cm^2 per pulse.

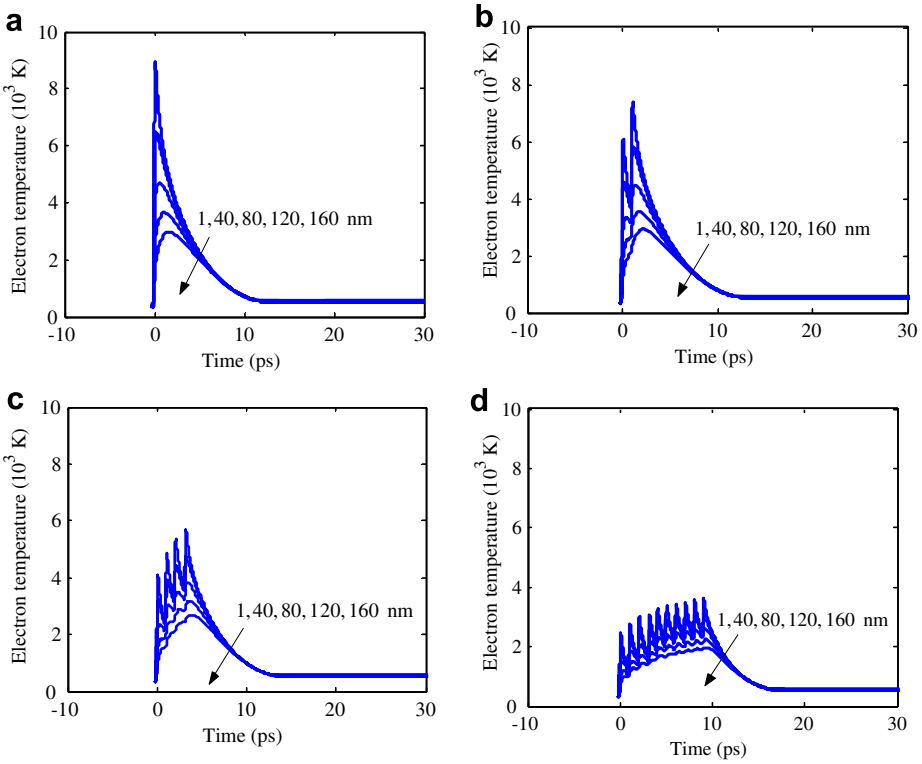

Fig. 3. Center ($r = 0$) electron temperatures at different depths (single burst; pulse separation = 1 ps): (a) single pulse per train at 0.1 J/cm^2 per pulse; (b) 2 pulses per train at 0.05 J/cm^2 per pulse; (c) 4 pulses per train at 0.025 J/cm^2 per pulse; (d) 10 pulses per train at 0.01 J/cm^2 per pulse.

The lattice temperatures at several sampling instants as a function of the thin film depth are given in Fig. 4. The highest lattice temperatures at the surface center ($r = 0$; $z = 1$ nm) are 557 K, 562 K, 568 K, and 571 K, respectively, for 1, 2, 4, and 10 pulses per train, while the lattice temperatures at the thin film bottom center ($z = 200$ nm) at

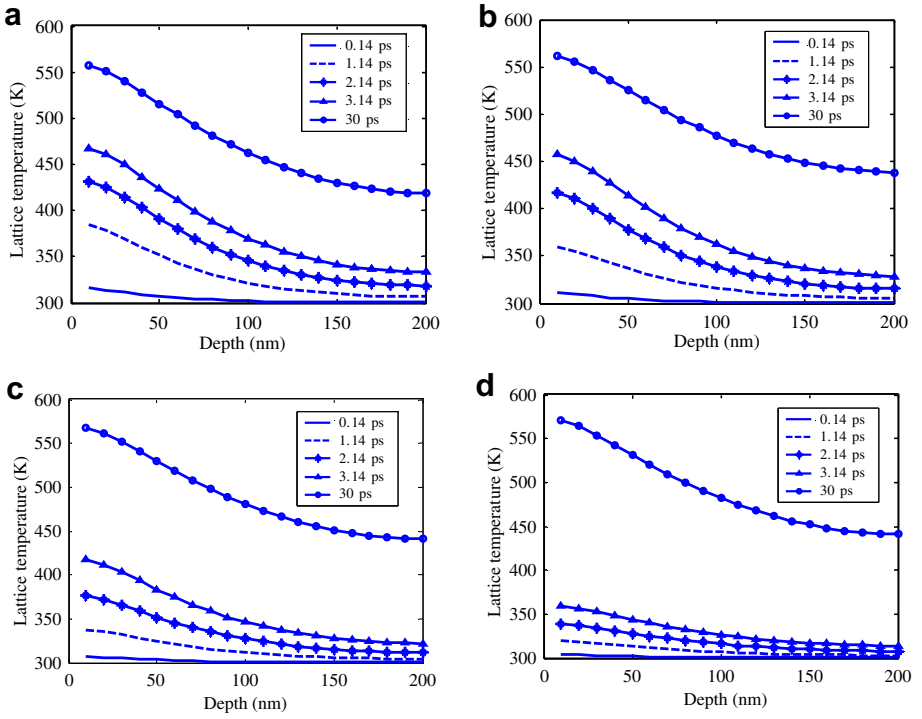

Fig. 4. Lattice temperatures ($r = 0$, $z = 1$ nm; single burst; pulse separation = 1 ps): (a) single pulse per train at 0.1 J/cm^2 per pulse; (b) 2 pulses per train at 0.05 J/cm^2 per pulse; (c) 4 pulses per train at 0.025 J/cm^2 per pulse; (d) 10 pulses per train at 0.01 J/cm^2 per pulse.

30 ps are 418 K, 438 K, 440 K, and 440 K, respectively. The thin film is heated to slightly higher temperatures by pulse trains, because the pulse(s) changes the optical properties (reflectivity and absorption coefficient) during the subsequent pulse irradiations. On the other hand, within the first three picoseconds, the lattice temperature in single pulse increases much faster than those in the pulse trains. At 3.14 ps, the surface temperatures are 467 K, 458 K, 417 K, and 358 K, respectively, for Cases (a)–(d), due to much higher transient electron temperatures in Case (a) at the same total energy per train.

3.2. Multiple bursts

The frequency (the reciprocal of the repetition rate) of a femtosecond laser (and its pulse trains) is typically a few Hz to tens of kHz. Hence, a burst period is on the order of 0.1 s to 0.1 ms, which is 10^8–10^{14} times longer than any femtosecond pulse duration. Within the burst period after the thermolization time (tens of picoseconds), the electrons and lattice have the same temperature, T_l, and the two-temperature model in this period can be simplified to

$$\frac{\partial T(t,r,z)}{\partial t} = \nabla(k\nabla T)/C(T) - \frac{\varepsilon_e \sigma[T^4(t,r,0) - T_0^4]}{C(T)d} \qquad (25)$$

where k is the heat conductivity; C is the heat capacity; T is the metal temperature; d is the film thickness, σ is the Stefan–Boltzmann constant, and ε_e is the emissivity taken as 0.03 [37]. The last term in Eq. (25) represents the radiation heat loss to the ambient, which could also be considered as the boundary condition.

The pulse energy and the pulse separation within the pulse train in this section are the same as those in Section 3.1. At a repetition rate 10 kHz, it takes 139, 133, 126, and 110 bursts, respectively, for 1, 2, 4, and 10 pulses per train to the melting temperature, 1337.33 K for gold. Hence, the pulse train technology can increase the photon efficiency in heating. In fact, this effect can be more effective for dielectrics [23,24] as compared to metals.

Due to the surface irradiation heat loss, the temperature change at $z = 1$ nm, $r = 0$ per burst cycle (including both burst irradiation and cooling between two bursts) decreases as a function of the burst number, which is depicted in Fig. 5 for the case of 10 pulses per train. The first burst cycle increases the center ($r = 0$) temperature by 28 K, while the 109th burst cycle increases it by only 3.7 K. Hence, at a 10 kHz frequency, surface radiation loss plays a significant role in the femtosecond laser heating of the metal thin film especially before the melting occurs. The surface lattice temperature increase per burst cycle in Cases (b)–(d) are very similar to that in Fig. 5 and, hence, they are omitted here.

3.3. Effects of repetition rate

As expected, the number of bursts required for melting decreases as the repetition rate increases as shown in Fig. 6. But at 10 of MHz to 100 of THz, (although currently the frequency of a femtosecond laser cannot be this high), the repetition rate has a negligible effect on the number of bursts required for metal melting in our simulation conditions. This shows that the thermal factors (lattice temperatures) dominate in pulse trains with millisecond to nanosecond train separation time, while the optical factors through electron temperature changes dominate in pulse trains with femtosecond-to-picosecond train separation time. It is also demonstrated that at 5 kHz, 308 and 227 bursts are required for melting by using 1 and 10 pulses per train, respectively, which confirms the photon-efficiency advantage of the pulse train due to the changes of the optical properties in the subsequent pulse(s). Considering the technology feasibility and cost, the repetition rate of 100 of kHz would be 'ideal' if the number of bursts required for metal melting is used as the target function.

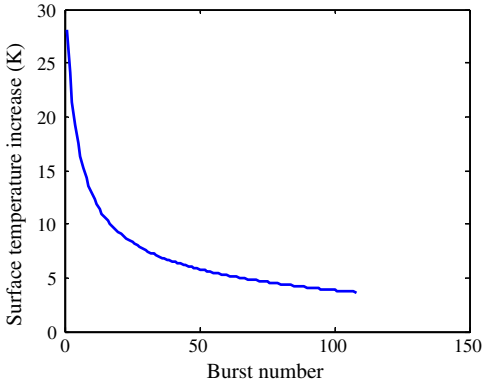

Fig. 5. Surface center ($r = 0$; $z = 1$ nm) lattice temperature increase per burst cycle.

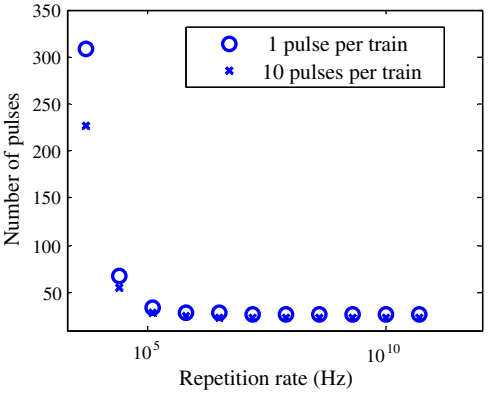

Fig. 6. Numbers of bursts needed for melting at different repetition rates (frequencies): single pulse per train at 0.1 J/cm^2 per pulse and 10 pulses per train at 0.01 J/cm^2 per pulse.

3.4. Pulse separation

An important parameter in the pulse train technology is the delay (separation) time between the two next pulses within a train, which is called the pulse separation. This

section studies the temperature responses under a single burst consisting of 3 pulses each at 0.1 J/cm^2 with the pulse separation of 0.5, 1, 2, 4, 8, and 16 ps, respectively, as shown in Fig. 7. The corresponding lattice temperatures after the thermolization time are: 1050, 1074, 1110, 1135, 1106, and 1088 K, respectively. Hence, the temperature right after the thermolization time first increases to a peak and then decreases as the pulse separation increases. This implies the existence of an optimum value of pulse separation time at which the metal heating (ablation) can be maximized by manipulating the temporal pulse distribution. There is no analytic method to directly calculate the optimal value of the pulse separation time. However, using the golden section search or simplex search, an optimal value with respect to a certain target function can be achieved.

With the pulse separation time of 0.5 ps or shorter, the three pulses are so close to each other and they act like a whole big pulse to excite electrons, which loses the major advantage of pulse trains. As the pulse separation increases, the three peaks of electron temperatures induced by the three pulses become obvious. However, when the pulse separation increases to the extent comparable to the single pulse thermolization time, (12 ps, which is different from the thermolization time of a pulse train), the electron responses induced by each pulse becomes independent to each other, which again loses the advantage of pulse trains.

4. Conclusions

This study uses the full-run quantum treatments to the two-temperature model for several critical optical and thermal properties, including the electron heat capacity, electron relaxation time, electron conductivity, reflectivity, and absorption coefficient. The improved two-temperature

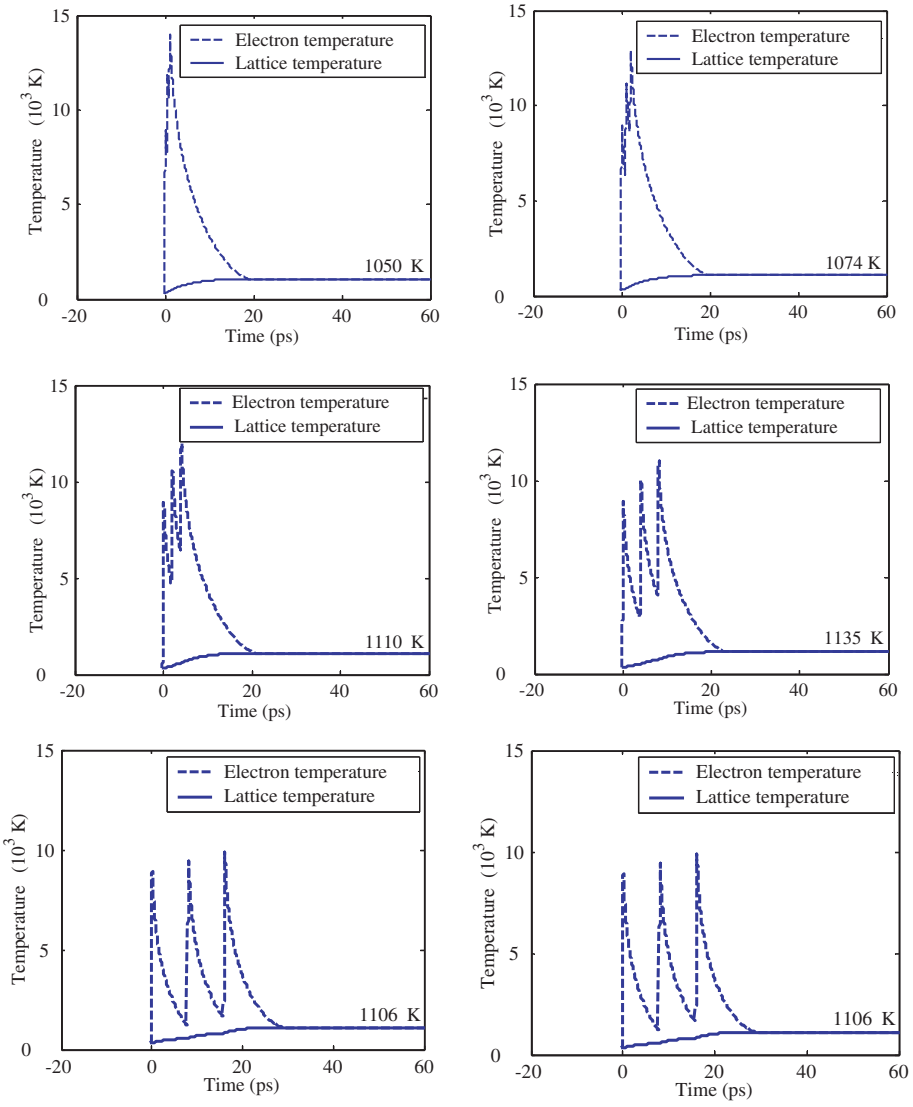

Fig. 7. Surface center ($r = 0$; $z = 1$ nm) temperatures of electrons and lattice under a single train consisting of three pulses at 0.1 J/cm^2 per pulse with the pulse separation of (a) 0.5 ps; (b) 1 ps; (c) 2 ps; (d) 4 ps; (e) 8 ps; and (f) 16 ps.

model is used to analyze the pulse train technology with the following major conclusions:

- *Pulse train technology*. The highest transient electron temperature (thus heat conductivity) is lowered and the thermolization time is prolonged by a pulse train, which preserves the advantages of ultrashort lasers, while it can reduce the problems associated with thermal cycles, such as stress-fracturing. The pulse train technology can increase the photon efficiency in melting (micromachining), which requires less number of pulses for melting.
- *Repetition rate*. The number of bursts required for melting decreases with the repetition rate. But at tens of MHz or higher, the repetition rate has a negligible effect on the number of bursts required for phase change.
- *Pulse separation*. The lattice temperature right after the thermolization time first increases to a peak and then decreases as the pulse separation increases. At a very short time separation, the pulses within a train are too close and act like a whole big pulse, which loses the major advantage of a pulse train. However, when the pulse separation increases to be comparable to the thermolization time of each single pulse, the electron responses induced by each pulse becomes independent to each other, which again loses the advantage of pulse trains.

Acknowledgements

This work was supported by the Air Force Research Laboratory under Contract No. FA8650-04-C-5704 and the National Science Foundation under Grant No. 0423233.

References

[1] B. Rethfeld, A. Kaiser, M. Vicanek, G. Simon, Ultrafast dynamics of nonequilibrium electrons in metals under femtosecond laser irradiation, Phys. Rev. B 65 (2002) 214303–214313.
[2] L. Jiang, H.L. Tsai, Improvements on two-temperature models and its applications in ultrashort laser damage of metal films, ASME J. Heat Transfer 127 (2005) 1167–1173.
[3] B.C. Stuart, M.D. Feit, S. Herman, A.M. Rubenchik, B.W. Shore, M.D. Perry, Optical ablation by high-power short-pulse lasers, J. Opt. Soc. Am. B 13 (1996) 459–468.
[4] R.W. Schoenlein, W.Z. Lin, J.G. Fujimoto, G.L. Eesley, Femtosecond studies of non-equilibrium electronic processes in metals, Phys. Rev. Lett. 58 (1987) 1680–1683.
[5] T.Q. Qiu, C.L. Tien, Short-pulse laser heating on metals, Int. J. Heat Mass Transfer 35 (1992) 719–726.
[6] T.Q. Qiu, C.L. Tien, Heat transfer mechanisms during short-pulse laser heating of metals, ASME J. Heat Transfer 115 (1993) 835–841.
[7] T.Q. Qiu, C.L. Tien, Femtosecond laser heating of multi-layer metals-I analysis, Int. J. Heat Mass Transfer 37 (1994) 2789–2797.
[8] T.Q. Qiu, T. Juhasz, C. Suarez, W.E. Bron, C.L. Tien, Femtosecond laser heating of multi-layer metals-II experiments, Int. J. Heat Mass Transfer 37 (1994) 2799–2808.
[9] D.Y. Tzou, J.K. Chen, J.E. Beraun, Hot-electron blast induced by ultrashort-pulsed lasers in layered media, Int. J. Heat Mass Transfer 45 (2002) 3369–3382.
[10] H.E. Elsayed-Ali, T.B. Norris, M.A. Pessot, G.A. Mourou, Time-resolved observation of electron–phonon relaxation in copper, Phys. Rev. Lett. 58 (1987) 1212–1215.
[11] T. Hertel, E. Knoesel, M. Wolf, G. Ertl, Ultrafast electron dynamics at Cu(1 1 1): response of an electron gas to optical excitation, Phys. Rev. Lett. 76 (1996) 535–538.
[12] B.R. Barron, W. Dai, A hybrid FE-FD scheme for solving parabolic two-step micro heat transport equations in an irregularly shaped three-dimensional double-layered thin film, Numer. Heat Transfer, B: Fundamentals 49 (5) (2006) 437–465.
[13] J.K. Chen, W.P. Latham, J.E. Beraun, Axisymmetric modeling of femtosecond-pulse laser heating on metal films, Numer. Heat Transfer, B: Fundamentals 42 (1) (2002) 1–17.
[14] J.K. Chen, J.E. Beraun, Numerical study of ultrashort laser–pulse interactions with metal films, Numer. Heat Transfer, A: Appl. 40 (1) (2001) 1–20.
[15] A.N. Smith, J.L. Hostetler, P.M. Norris, Non-equilibrium heating in metal films: an analytical and numerical analysis, Numer. Heat Transfer, A: Appl. 35 (8) (1999) 859–873.
[16] S.H. Lee, J.S. Lee, S. Park, Y.K. Choi, Numerical analysis on heat transfer characteristics of a silicon film irradiated by pico- to femtosecond pulse lasers, Numer. Heat Transfer, A: Appl. 44 (8) (2003) 833–850.
[17] B. Xu, B.Q. Li, Finite element solution of non-fourier thermal wave problems, Numer. Heat Transfer, Part B: Fundamentals 44 (1) (2003) 45–60.
[18] R. Bartels, S. Backus, E. Zeek, L. Misoguti, G. Vdovin, I.P. Christov, M.M. Murnane, H.C. Kapteyn, Shaped-pulse optimization of coherent emission of high-harmonic soft X-rays, Nature 406 (2000) 164–166.
[19] A. Lindinger, C. Lupulescu, M. Plewicki, F. Vetter, A. Merli, M.S. Weber, L. Wöste, Isotope selective ionization by optimal control using shaped femtosecond laser pulses, Phys. Rev. Lett. 93 (2004) 033001–033004.
[20] M. Renard, E. Hertz, B. Lavorel, O. Faucher, Controlling ground-state rotational dynamics of molecules by shaped femtosecond laser pulses, Phys. Rev. A 69 (2004) 043401–043406.
[21] A. Assion, T. Baumert, M. Bergt, T. Brixner, B. Kiefer, V.V. Seyfried, M. Strehle, G. Gerber, Control of chemical reactions by feedback-optimized phase-shaped femtosecond laser pulses, Science 282 (1998) 919–922.
[22] A.A. Andreev, J. Limpouch, A.B. Iskakov, H. Nakano, Enhancement of X-ray line emission from plasmas produced by short high-intensity laser double pulses, Phys. Rev. E 65 (2002) 026403–026411.
[23] L. Jiang, H.L. Tsai, Repeatable nanostructures in dielectrics by femtosecond laser pulse trains, Appl. Phys. Lett. 87 (2005) 151104–151106.
[24] R. Stoian, M. Boyle, A. Thoss, A. Rosenfeld, G. Korn, I.V. Hertel, E.E.B. Campbell, Laser ablation of dielectrics with temporally shaped femtosecond pulses, Appl. Phys. Lett. 80 (2002) 353–355.
[25] M. Spyridaki, E. Koudoumas, P. Tzanetakis, C. Fotakis, R. Stoian, A. Rosenfeld, I.V. Hertel, Temporal pulse manipulation and ion generation in ultrafast laser ablation of silicon, Appl. Phys. Lett. 83 (2003) 1474–1476.
[26] E. Ohmaru, T. Okamoto, S. Fujiwara, T. Sano, I. Miyamoto, Chromium thin film ablation with double pulse of femtosecond laser, In: Proceeding of International Congress on Applications of Laser & Electro-Optics, Miami, FL, 2004.
[27] M. Lapczyna, K.P. Chen, P.R. Herman, H.W. Tan, R.S. Marjoribanks, Ultra high repetition rate (133 MHz) laser ablation of aluminum with 1:2-ps pulses, Appl. Phys. A 69 (Suppl.) (1999) S883–S886.
[28] I.H. Chowdhury, X.F. Xu, A.M. Weiner, Ultrafast pulse train micromachining, Commercial and Biomedical Applications of Ultrafast Lasers III, Proc. SPIE 4978 (2003) 138–146.

[29] N.W. Ashcroft, N.D. Mermin, Solid State Physics, Holt, Rinehart, and Winston, New York, 1976.
[30] E.G. Gamaly, A.V. Rode, B. Luther-Davies, V.T. Tikhonchuk, Ablation of solids by femtosecond lasers: ablation mechanism and ablation thresholds for metals and dielectrics, Phys. Plas. 9 (2002) 949–957.
[31] Y.T. Lee, R.M. More, An electron conductivity model for dense plasma, Phys. Fluids 27 (5) (1984) 1273–1286.
[32] L. Jiang, H.L. Tsai, Prediction of crater shape in femtosecond laser ablation of dielectrics, J. Phys. D 37 (2004) 1492–1496.
[33] L. Jiang, H.L. Tsai, Energy transport and material removal during femtosecond laser ablation of wide bandgap materials, Int. J. Heat Mass Transfer 48 (2005) 487–499.
[34] M. Fox, Optical Properties of Solids, Oxford University Press, Oxford, 2001.
[35] G.L. Eesley, Generation of non-equilibrium electron and lattice temperatures in copper by picosecond laser pulses, Phys. Rev. B 33 (1986) 2144–2151.
[36] B. Palpant, B. Prével, J. Lermé, E. Cottancin, M. Pellarin, Optical properties of gold clusters in the size range 2–4 nm, Phys. Rev. B 57 (1998) 1963–1970.
[37] Y.A. Cengel, Heat Transfer: A Practical Approach, McGraw-Hill, Boston, MA, 1998.